Valence transition theory of the pressure-induced dimensionality crossover in superconducting $Sr_{14-x}Ca_xCu_{24}O_{41}$

Jeong-Pil Song [1], R. Torsten Clay,[2] and Sumit Mazumdar [1,*]
[1]*Department of Physics, University of Arizona, Tucson, Arizona 85721, USA*
[2]*Department of Physics and Astronomy, and HPC² Center for Computational Sciences, Mississippi State University, Mississippi 39762, USA*

(Received 2 August 2022; revised 2 October 2023; accepted 11 October 2023; published 23 October 2023)

One of the strongest justifications for the continued search for superconductivity within the single-band Hubbard Hamiltonian originates from the apparent success of single-band ladder-based theories in predicting the occurrence of superconductivity in the cuprate coupled-ladder compound $Sr_{14-x}Ca_xCu_{24}O_{41}$. Recent theoretical works have, however, shown the complete absence of quasi-long-range superconducting correlations within the hole-doped multiband ladder Hamiltonian including realistic Coulomb repulsion between holes on oxygen sites and oxygen-oxygen hole hopping. Experimentally, superconductivity in $Sr_{14-x}Ca_xCu_{24}O_{41}$ occurs only under pressure and is preceded by dramatic transition from one to two dimensions that remains not understood. We show that understanding the dimensional crossover requires adopting a valence transition model within which there occurs transition in Cu-ion ionicity from +2 to +1, with transfer of holes from Cu to O ions [S. Mazumdar, Phys. Rev. B **98**, 205153 (2018)]. The driving force behind the valence transition is the closed-shell electron configuration of Cu^{1+}, a feature shared by cations of all oxides with a negative charge-transfer gap. We make a falsifiable experimental prediction for $Sr_{14-x}Ca_xCu_{24}O_{41}$ and discuss the implications of our results for layered two-dimensional cuprates.

DOI: 10.1103/PhysRevB.108.134510

I. INTRODUCTION

Theoretical efforts to elucidate the mechanism of superconductivity (SC) in the cuprates have been overwhelmingly within the one-band Hubbard Hamiltonian. Multiple recent demonstrations of nonsuperconducting ground state within the optimally doped two-dimensional (2D) Hubbard model with nearest-neighbor particle hoppings [1–3] have led to subsequent search for superconductivity within single-band correlated-electron Hamiltonians that include next-nearest-neighbor [4–6] and even longer range hopping [7]. These approaches have also failed to find long-range superconducting correlations with hole doping (see, however, Ref. [8]). Theoretical models that treat the one-band 2D lattice as weakly coupled two-leg ladders [9,10] are considered promising, given the presence of quasi-long-range (quasi-LR) superconducting correlations in the two-leg one-band ladder [11–15]. Observation of SC in $Sr_{14-x}Ca_xCu_{24}O_{41}$ (SCCO) for $10 \leqslant x \leqslant 13.6$ [16–19], consisting of weakly coupled Cu_2O_3 ladders, is often interpreted as confirmation of the one-band ladder-based theories [11–15].

The failure of single-band model calculations to find SC in the layered systems and yet their apparent success in explaining experimentally observed SC in SCCO, taken together, are mysterious. We therefore performed density matrix renormalization group (DMRG) calculations to test whether or not quasi-LR superconducting correlations persisted within a multiband ladder Hamiltonian [20,21]. Our calculations found the same doping asymmetry detected in single-band calculations in 2D [4–7], viz., the complete absence of quasi-LR superconducting correlations on hole-doping for realistic Coulomb repulsion of holes on O ions and O-O hole hopping [20,21], and SC persisting even at large doping concentrations on the electron-doped side [21]. The rapid decays of the spin gap as well as superconducting pair correlations in the hole-doped multiband ladder [21] are caused by the the strong pair-breaking effect due to O-O hopping. Significant departure from "traditional" approaches is therefore necessary to understand the experimental observations in SCCO. We believe that the experimental observations of one-to-two dimensional (1D-to-2D) transition in SCCO (see below) is a clear signature of a valence transition mechanism for superconducting cuprates formulated recently [22]. We examine this issue in detail in this paper. Our approach has strong parallels with valence instability theories of the physics of heavy-fermion systems [23–26] and provides a broad framework for understanding "negative charge-transfer gap" materials that are of considerable recent interest [27–33].

Multiple experimental research groups have maintained that SC in SCCO is 2D and is likely outside the scope of ladder-based theories [11–15]. SC in SCCO results not from mere substitution of Sr with Ca in $Sr_{14}Cu_{24}O_{41}$, but is pressure driven [17–19,34,35]. At $x = 11.5$ SC is realized under pressure $P = 3.5$–8 GPa, with maximum superconducting $T_c = 9$ K at 4.5 GPa. The ambient pressure resistivity ρ_c along the ladder leg direction (c axis) decreases with temperature at ambient pressure for temperature $T > 80$ K, with an upturn

*Corresponding author: mazumdar@arizona.edu

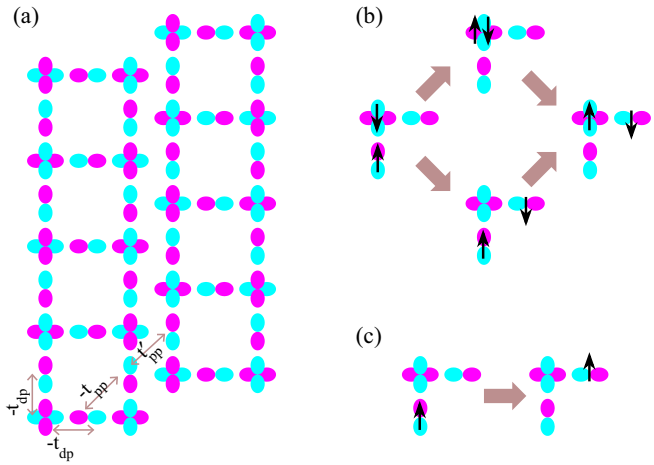

FIG. 1. (a) Schematic of the coupled two-leg multiband Cu_2O_3 ladders investigated numerically. Intraladder (t_{dp}, t_{pp}) and interladder (t'_{pp}) hopping parameters are indicated. (b) Intraladder hole hopping between leg oxygen O_L and rung oxygen O_R at ambient pressure involving the hole on the Cu ion. (c) Direct intraladder hole hoppings between O ions without involving the hole on the Cu ion. The hole occupancy of the Cu ion in this case is irrelevant.

at lower T. The resistivity ρ_a along the ladder rung direction (a axis) is incoherent even at high T at ambient pressure. This changes dramatically for $P > P_c = 3.5$ GPa in the state immediately preceding SC; here ρ_c is metallic at all T, its magnitude at 300 K being nearly one-third of that at ambient pressure. The decrease in ρ_a is even more dramatic for $P > P_c$. ρ_a/ρ_c drops by a factor of ∼4–5 at T near 50 K, where a maximum in this ratio occurs at ambient pressure. The pressure-induced SC is an insulator-superconductor (I-SC) transition that has remarkable similarity with the SC-I transition in 2D cuprates under Zn substitution of Cu, in that the "average resistivity" $(\rho_c\rho_a)^{1/2}$ of SCCO immediately prior to SC is the universal 2D resistivity [17] $h/4e^2$ characteristic of 2D SC-I transitions [36].

Experimental determination of nonzero spin gap Δ_s for all x in SCCO [19] is cited in support of one-band ladder theories [11,12]. NMR measurements, however, consistently reported the appearance of gapless spin excitations [19,34,35,37] at the superconducting composition for $P \geqslant P_c$. Pressure-dependent measurement of relaxation time T_1 has found that Δ_s is pressure independent until P_c is reached, following which it suddenly approaches zero exactly as there occurs a large jump in the superconducting T_c [35]. Taken together, the observation of universal 2D resistance [17] and $\Delta_s \to 0$ indicate a true phase transition at $P = P_c$.

Experimental research groups have conjectured that pressure-driven hole transfer from the CuO_2 chains to the Cu_2O_3 ladders is behind the two-dimensionality and vanishing of Δ_s [18,19,38,39]. The extent of hole transfer from chains to ladders, caused by Ca substitution of Sr, is small [40]. Whether or not pressure-induced additional hole-transfer by itself is sufficient to lead to two-dimensionality has not been probed theoretically.

We report here DMRG calculations (see Supplemental Material (SM), S.1 [41] and references [42,43] therein) of intraladder versus interladder coupling strengths for coupled Cu_2O_3 ladders within a multiband Hubbard model. The 90° Cu-O-Cu interladder linkage implies that the effective interladder Cu-Cu hopping integral is tiny [18,44]. The absence of noticeable deformation of the ladder structure up to 9 GPa [18] indicates that the interladder Cu-Cu coupling continues to be weak under pressure. Interladder coupling therefore originates from hole hopping between O ions occupying different ladders. The possibility then exists that inclusion of realistic O-O hopping [45] might indeed find increased two-dimensionality with increased doping. We show conclusively that pressure-driven increased hole concentration in the ladders, *which has no other consequence*, fails to reproduce the observed increase in effective dimensionality. We then show that two-dimensionality can be understood only within the proposed valence transition theory of layered cuprates [22], wherein the insulator-to-conductor transition is driven by a sharp decrease in Cu-ion ionicity from nearly +2 to nearly +1. Nearly all holes, including the ones previously occupying the Cu $d_{x^2-y^2}$ orbitals, now occupy the 2D O sublattice.

Valence transition has been widely discussed in the context of neutral-to-ionic transition in organic charge-transfer solids [46–50] and in heavy-fermion materials [23–26]. Following valence transition, cuprates have a negative charge-transfer gap, meaning that charge-transfer absorption in the ground state involves hole transfer from the O anion to the Cu cation and not the other way around. One hole is transferred from Cu to the O sublattice, giving an average hole density of one-half hole per O atom. The system now behaves as a nearly $\frac{1}{4}$-filled 2D O band of interacting holes, with the closed-shell Cu^{1+} ions playing a negligible role.

In what follows we develop our theory and present the results of our DMRG calculations in steps. In Sec. II we present the multiple-band model Hamiltonian for coupled Cu_2O_3 ladders. Section III A reports computational results within the Hamiltonian for standard parameters. It is shown that the standard model fails to explain the experimentally observed 1D-to-2D transition. The obvious implication is that SC in SCCO is therefore not currently understood. Theoretical models that consider layered cuprates as coupled ladders [9,10] therefore do not resolve the impasse [1–7] the field of cuprate SC is facing. We then present the physical arguments behind the valence transition mechanism that are essential for understanding the dimensional crossover (Sec. III B) and follow up with explicit calculations (Secs. III C and III D). Finally, in Sec. IV we present our conclusions, where we arrive to our key argument that doped cuprates are prime candidates for being in the negative charge-transfer gap category. In the Appendix we discuss the current knowledge base on oxides that are known to have negative charge-transfer gaps, emphasizing in particular a central feature that is common to the cationic components of all such compounds, and how that feature is shared by cuprates. Additional data are available in the Supplemental Material [41].

II. COUPLED LADDER MODEL

In Fig. 1(a) we show the schematic of the coupled multiband ladders we consider. The Hamiltonian is

written as

$$
\begin{aligned}
H = \Delta_{\rm dp} \sum_{\mu,i,\sigma} p^{\dagger}_{\mu,i,\sigma} p_{\mu,i,\sigma} - \sum_{\mu,\lambda,\langle ij\rangle,\sigma} t_{\rm dp} (d^{\dagger}_{\mu,\lambda,i,\sigma} p_{\mu,j,\sigma} + {\rm H.c.}) \\
- \sum_{\mu,\langle ij\rangle,\sigma} t_{\rm pp} (p^{\dagger}_{\mu,i,\sigma} p_{\mu,j,\sigma} + {\rm H.c.}) \\
- \sum_{\mu\neq\mu',\langle ij\rangle,\sigma} t'_{\rm pp} (p^{\dagger}_{\mu,i,\sigma} p_{\mu',j,\sigma} + {\rm H.c.}) \\
+ U_{\rm d} \sum_{\mu,\lambda,i} d^{\dagger}_{\mu,\lambda,i,\uparrow} d_{\mu,\lambda,i,\uparrow} d^{\dagger}_{\mu,\lambda,i,\downarrow} d_{\mu,\lambda,i,\downarrow} \\
+ U_{\rm p} \sum_{\mu,j} p^{\dagger}_{\mu,j,\uparrow} p_{\mu,j,\uparrow} p^{\dagger}_{\mu,j,\downarrow} p_{\mu,j,\downarrow}. \qquad (1)
\end{aligned}
$$

Here $d^{\dagger}_{\mu,\lambda,i,\sigma}$ creates a hole with spin σ on the ith Cu $d_{x^2-y^2}$ orbital on the λth leg ($\lambda = 1$ and 2) of the μth ladder ($\mu = 1$ and 2); $p^{\dagger}_{\mu,j,\sigma}$ creates a hole on the rung oxygen O_R or leg oxygen O_L; $t_{\rm dp}$ are nearest-neighbor (n.n.) intraladder rung and leg Cu-O hopping integrals, and $t_{\rm pp}$ and $t'_{\rm pp}$ are n.n. intra- and interladder O-O hopping integrals, respectively [Fig. 1(a)]. $U_{\rm d}$ and $U_{\rm p}$ are the on-site repulsions on the Cu and O sites.

First-principles calculations of the parameters for the undoped 2D insulating compounds [45] found $U_{\rm d} = 8$, $U_{\rm p} = 3$, $t_{\rm pp} = 0.5$, and $\Delta_{\rm dp} = 3$ in units of $t_{\rm dp}$, close to other calculations. $\Delta_{\rm dp}$ is assumed in nearly all existing theoretical work as a fundamental quantity that is the difference between one-electron site energies of Cu and O ions. Based on explicit discussions in the context of neutral-to-ionic transition [46–50] and heavy fermions [25,26], we argue that over and above one-electron atomic quantities, $\Delta_{\rm dp}$ also depends on long-range many-body interactions that are strongly carrier-concentration dependent (see below) [22,51–53]. Determination of precise doping-concentration dependence of $\Delta_{\rm dp}$ is outside the scope of first-principles calculations and therefore has not been attempted. Semiquantitative estimates of $\Delta_{\rm dp}$ can, however, be made from comparisons against known reference compounds. For example, experimentally, Δ_s in SCCO for $x = 12$ [35] is smaller than that in $SrCu_2O_3$ [54] by a factor of 4–5. Presumably this is due to the completely undoped nature of $SrCu_2O_3$ and a small nonzero hole concentration in the ladder layer of SCCO. Δ_s is nearly the same for undoped single and coupled ladders (S.2, Fig. S2 [41]), but decreases rapidly with $\Delta_{\rm dp}$. Assuming $\Delta_{\rm dp}$ in $SrCu_2O_3$ is comparable to that in 2D cuprates, we conclude that for SCCO at ambient pressure $\Delta_{\rm dp} \sim 1.0$–2.0.

III. COMPUTATIONAL RESULTS

A. Failure of the standard model

We measure effective dimensionalities from bond orders, which are expectation values of charge transfers between ions. Bond orders, though not direct measures of dc resistivity, measure the electronic kinetic energy in any direction and are related by the sum rule to the frequency-dependent optical conductivity. We calculate, (i) the n.n. Cu-O bond order $B^{\rm Cu\text{-}O}_{\rm leg}$ along the ladder legs at the interface of the two ladders, $\langle \sum_\sigma d^{\dagger}_{\mu,\lambda,i,\sigma} p_{\mu,j,\sigma} + {\rm H.c.}\rangle$, (ii) the intraladder bond order $B^{\rm O\text{-}O}_{\rm intra}$ between n.n. O_R and O_L, $\langle \sum_\sigma p^{\dagger}_{\mu,i,\sigma} p_{\mu,j,\sigma} + {\rm H.c.}\rangle$, and (iii) the interladder bond order $B^{\rm O\text{-}O}_{\rm inter}$, $\langle \sum_\sigma p^{\dagger}_{\mu,i,\sigma} p_{\mu',j,\sigma} + {\rm H.c.}\rangle$, where $\mu \neq \mu'$ and i and j are n.n. We also calculated n.n.n. bond orders along the ladder legs at the interface of the two ladders, $B^{\rm Cu\text{-}Cu}_{\rm leg} = \langle \sum_\sigma d^{\dagger}_{\mu,\lambda,i,\sigma} d_{\mu,\lambda,i+1,\sigma} + {\rm H.c.}\rangle$ and $B^{\rm O\text{-}O}_{\rm leg} = \langle \sum_\sigma p^{\dagger}_{\mu,i,\sigma} p_{\mu,j,\sigma} + {\rm H.c.}\rangle$. Our DMRG computations are for coupled ladders consisting of 8 and 12 Cu-O-Cu rungs (hereafter 8×2 and 12×2 ladders), consisting of 76 and 116 total ions, respectively, with open boundary conditions along both ladder leg and rung directions. Bond orders being single-particle operators exhibit negligible finite-size effects (see Sec. S.3, Tables I and II, and Fig. S4 [41]).

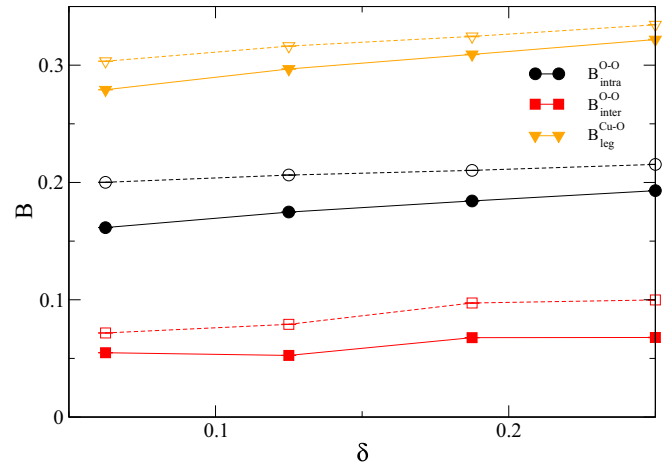

FIG. 2. Calculated bond orders B (see text) for $\Delta_{\rm dp} = 1$ (dashed lines) and $\Delta_{\rm dp} = 2$ (solid lines) versus hole doping δ in the 8×2 coupled ladder with $t'_{\rm pp} = 0.5$.

We first test the simple conjecture that increase in effective dimensionality is a consequence of hole transfer alone from chains to ladders [18,19,38,39]. We consider dopings δ, where $1 + \delta$ is the average hole concentration per Cu ion ($\delta = 0$ for the undoped ladders). In Fig. 2 we show bond orders for the 8×2 coupled ladder, for $\Delta_{\rm dp} = 1$ and 2. $B^{\rm Cu\text{-}O}_{\rm leg}$ and $B^{\rm O\text{-}O}_{\rm intra}$, taken together (but not simply additively), measure intraladder hole transport, while $B^{\rm O\text{-}O}_{\rm inter}$ measures interladder transport. For both $\Delta_{\rm dp}$ all bond orders exhibit rather weak increase with δ. For $\delta \leqslant 0.125$ the small increases in intraladder bond orders $B^{\rm Cu\text{-}O}_{\rm leg}$ and $B^{\rm O\text{-}O}_{\rm intra}$ with δ are relatively more significant than the increase in $B^{\rm O\text{-}O}_{\rm inter}$. Our results in this region of δ are in agreement with the conclusion in Ref. [18], viz., increased δ increases anisotropy and not otherwise. In Sec. S.3 [41] we have presented partial results of calculations of the bond orders for $t'_{\rm pp} = 0.3$, for which the interladder O-O bond order also remains almost δ independent. The very large pressure-driven decrease [17] in ρ_a/ρ_c at low T thus cannot be understood within the hole-transfer conjecture [18,19,38,39].

An interesting feature of Fig. 2 is the much larger $B^{\rm O\text{-}O}_{\rm intra}$ relative to $B^{\rm O\text{-}O}_{\rm inter}$, for both $\Delta_{\rm dp}$. This larger magnitude is ascribed to the additional paths via Cu ions that holes can take when hopping from O_L-to-O_R of the same ladder. In Figs. 1(b) and 1(c) we give the schematics of the intraladder O_R-to-O_L hole transfers, involving and not involving the hole on the Cu-ion, respectively. The much larger calculated $B^{\rm O\text{-}O}_{\rm intra}$ in Fig. 2 implies that hole transfers via paths in Fig. 1(b) dominate

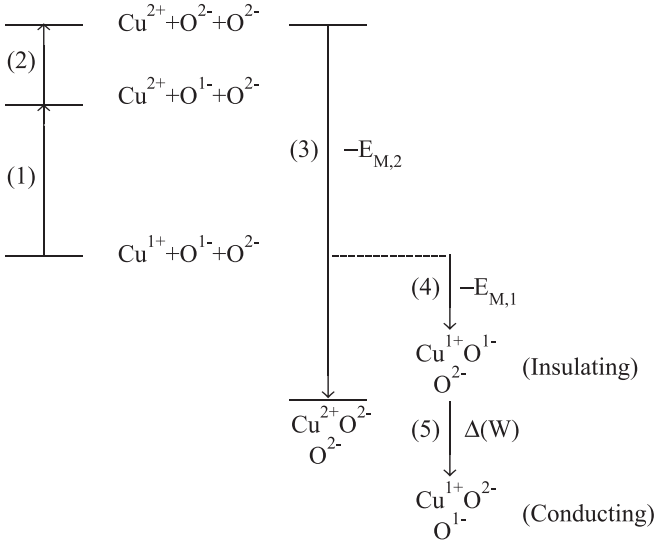

FIG. 3. Schematic diagram of the competition between the two distinct ground states. The vertical axis depicts energy.

overwhelmingly over the path in Fig. 1(c). Bond orders and the true interladder coupling strengths therefore depend not only on the magnitudes of the hopping integrals but also on the charge density of the ions involved. In Sec. S.4, Tables III and IV [41], we give the Cu and O ion charges for both Δ_{dp}. The very small O-ion charges explain the small magnitudes of $B_{inter}^{O\text{-}O}$.

B. Valence transition and negative Δ_{dp}

It follows that two dimensionality requires substantial increase in hole population on the O sublattice, which is intrinsically 2D unlike the Cu sublattice. This can only originate from significant change in Δ_{dp}, including even change of sign which would correspond to transition from positive to negative charge-transfer gap. A negative charge-transfer gap has been found in several different materials, based largely on extensions to DFT [27,28,30–33] (see the Appendix). Here we approach it from the ionic limit, which allows easier visualization of the boundary between positive and negative charge-transfer [46–48]. Negative charge-transfer requires that the transition metal cation M can exist in two stable proximate oxidation states, usually M^{n+} and $M^{(n-1)+}$. When the energies of these two states are close, transitions between the two can be driven by tuning parameters like temperature or pressure. We argue that this is most likely when the ionization energy of $M^{(n-1)+}$ is unusually large (see Ref. [41], Sec. S.5).

Figure 3 gives a qualitative understanding of the boundary between positive and negative charge-transfer gap in the context of cuprates. We compare the relative energies of formation of two different extreme states, both with the same overall charge on the ionic unit cell $[CuO_2]^{2-}$, starting from the same initial state, consisting of isolated Cu^{1+}, O^{1-}, and O^{2-} ions. One of the the final states is the "usual" one with Cu-ion charge 2+ and both O ions with charge 2−. There exists a competing configuration where the charge on Cu is 1+, and one of the O ions has charge 1−. The latter is the negative charge-transfer gap state. It is understood that the ionic charge 2− on the unit cell is balanced by other components of the crystal. It is also assumed that the system has a few additional holes on the O sublattice in some of the $[CuO_2]^{2-}$ units, as would occur in the so-called Emery model, but these are not essential for our discussion.

Figure 3 gives the various steps through which the final states are arrived at, starting from isolated ions. Creating Cu^{2+} requires the second ionization energy of Cu, I_2 (step 1 in Fig. 3). As shown in Fig. S6(c) [41], I_2 for Cu is significantly larger than usual because of the closed-shell nature of Cu^{1+}. Additional energy is required to convert O^{1-} to O^{2-}, as the second electron affinity of O, A_2, is positive. These energy inputs create the free cation Cu^{2+} and two free O^{2-} anions, which are at very high energy relative to the initial state. Madelung energy $E_{M,2}$ is gained, however, in step 3, as the ions are brought together. The overall system has energy below the initial state with free ions and the state is therefore stable. As indicated in Fig. 3, the alternate state $[Cu^{1+}O^{2-}O^{1-}]^{2-}$ is arrived at from the initial state with a smaller Madelung energy gain $E_{M,1}$ (step 4). In cuprates and other oxides where the number of anions is larger than the number of cations, this alternate state with charge carriers occupying a non-half-filled band of anions is conducting. This is step 5 in the schematic, where additional energy gain occurs due to charge carrier delocalization. Collecting the energy differences gives the inequality [22]

$$I_n + A_2 + \Delta E_{M,n} + \Delta(W) \gtrless 0, \tag{2}$$

where I_n is the nth ionization energy of M ($M^{(n-1)+} \rightarrow M^{n+} + e$). $\Delta E_{M,n} = E_{M,n} - E_{M,n-1}$, where $E_{M,n}$ and $E_{M,n-1}$ are the per cation Madelung energies of the solid with the cation charges of $+n$ and $+(n-1)$, respectively. $\Delta(W) = W_n - W_{n-1}$, where W_n and W_{n-1} are the per cation gains in one-electron delocalization (band) energies of states with cationic charges $+n$ and $+(n-1)$, respectively. The larger right-hand (left-hand) side favors M^{n+} ($M^{(n-1)+}$) with positive (negative) charge-transfer gap. Distinct near-integer oxidation states, as opposed to mixed valence requires that the two largest terms in Eq. (2), I_n and $|\Delta E_{M,n}|$, are much larger than $|t_{dp}|$, even as the overall charge-transfer gap is comparable to $|t_{dp}|$ [46–50]. This is true in the cuprates where I_2 and $|\Delta E_{M,n}|$ are close to several tens of eV and $|t_{dp}| \sim 1$ eV.

Equation (2) has seen extensive applications in the context of neutral-to-ionic transition in organic charge-transfer solids, where due to effective one-dimensionality of the crystals the transition is between insulating states [48]. However, in this case, because one of the two oxidation states being compared is metallic, the concept of fixed doping-induced "site energies" is erroneous, as $E_{M,1}$, $E_{M,2}$, and $\Delta(W)$ are all strongly carrier-concentration dependent. The relative energies of the final states with two ionicities cannot be easily determined from first-principles calculations, and comparing with experiments is the only route to arriving at the correct semiempirical Hamiltonian.

Within our theory, SCCO at ambient pressures is correctly described within the standard picture of weakly coupled two-leg ladders with Cu^{2+} ions at the vertices and positive Δ_{dp}. The a-axis resistivity is incoherent because of the very small density of holes on O sites. The system is, however, close to

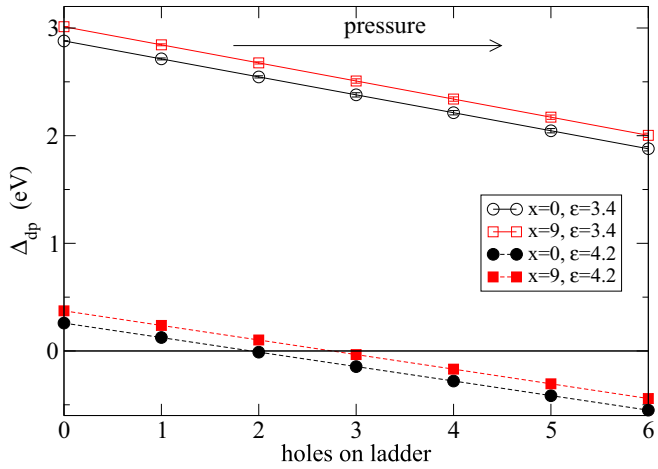

FIG. 4. Δ_{dp} versus the number of holes per formula unit on the ladders calculated from Eq. (3) (see text). Open (solid) symbols are calculated assuming the dielectric constant ϵ is 3.4 (4.2). Lines are guides to the eye. As indicated by the arrow, pressure increases the hole density on ladders, resulting in a decrease in Δ_{dp}.

the boundary between positive and negative charge-transfer gaps defined by Eq. (2).

C. Pressure-driven valence transition

We next seek to explain why pressure would drive a $Cu^{2+} \rightarrow Cu^{1+}$ valence transition in SCCO. Pressure-driven hole transfer from chains to ladders, over and above the transfer driven by Ca substitution, has indeed been observed experimentally [35,39,55,56]. Hole concentration in the ladder likely jumps from nearly 1 at ambient pressure to about 4 at $P > P_c$ per formula unit [55]. This has strong consequences on the magnitude and the even sign of Δ_{dp}. In the ionic limit [51],

$$\Delta_{dp} = \frac{e\Delta V_{\text{Cu-O}}}{\epsilon} - I_2 - A_2 - \frac{e^2}{d}. \tag{3}$$

In Eq. (3), $\Delta V_{\text{Cu-O}}$ is the difference in Madelung site potentials between ladder oxygen and copper sites, ϵ is the high-frequency dielectric constant, and d is the Cu-O distance. In insulating 2D cuprates $\Delta_{dp} \approx$ 2–3 eV; the first term $\Delta V_{\text{Cu-O}}/\epsilon$ is a positive quantity and $-I_2 - A_2 - \frac{e^2}{d} \approx -10.9$ eV [51,57]. Reference [57] assumed $\epsilon = 3.4$ for SCCO (see below). Pressure and doping enter Eq. (3) in three ways. First, changes in the lattice structure directly influence the Madelung potentials. Second, as noted above, with doping and pressure, holes are transferred from chains to ladders. Third, changes in the electronic structure will affect ϵ.

The first two effects are straightforward to calculate. We calculated Madelung site potentials for a unit cell containing 4 formula units of SCCO using standard Ewald methods with the GULP software package [58–61] and the crystal structure reported in Ref. [62] for the $x = 0$ and $x = 9$ compounds. We assumed the ionic charges of Sr/Ca and Cu are 2+. We assumed all oxygen ions were O^{2-}, and then randomly introduced holes (O^{1-}) on chain or ladder O sites. Figure 4 shows the average Δ_{dp} calculated from 100 random hole distributions for each relative chain/ladder hole occupation. If we assume an increase of three to four holes per formula unit under doping and pressure (see Ref. [55]), this gives a net decrease of ≈0.7 eV in Δ_{dp}.

In Fig. 4 our first set of points assumes $\epsilon = 3.4$ as in Ref. [57]. Because $\Delta V_{\text{Cu-O}}$ is large (∼45 eV), small changes in ϵ lead to large changes in Δ_{dp}. An increase in carrier density would increase metallicity-induced electronic screening, reducing Δ_{dp}. For example, in superconducting Bi-2212 samples, $3.5 \lesssim \epsilon \lesssim 4.3$ (see Table 2 in Ref. [63]). With $\epsilon \approx 4.2$, our calculated Δ_{dp} reaches 0 with three holes transferred to the ladder layer and negative values for larger number of holes transferred (see Fig. 4). In reality, ϵ should be treated as a function of doping, $\epsilon(\delta)$, leading to transition from positive to negative Δ_{dp}. Δ_{dp} must be calculated self-consistently within the many-body electronic state of the system. Following valence transition there is a gain in delocalization energy as the system changes from a nearly half-filled, quasi-one-dimensional copper-based Mott-Hubbard state to a two-dimensional nearly quarter-filled oxygen-band metal. This increase in conductivity would act to further decrease Δ_{dp} through its dependence on $\epsilon(\delta)$.

D. Dimensional crossover

We now reconsider the results of Sec. III A, allowing for the possibility that $\Delta_{dp} < 0$. In Fig. 5(a) we plot the same bond orders as in Fig. 2, along with n.n.n. $B_{\text{leg}}^{\text{Cu-Cu}}$ and $B_{\text{leg}}^{\text{O-O}}$, for 12×2 coupled ladders, now as a function of Δ_{dp} for fixed $\delta = 0.125$, for $t'_{pp} = 0.5$. These results are in sharp contrast with those of Fig. 2. $B_{\text{intra}}^{\text{O-O}}$ and $B_{\text{inter}}^{\text{O-O}}$ both now increase as Δ_{dp} goes from positive to negative, simulating the decrease of ρ_c and ρ_a with pressure. In Fig. 5(b) we plot the ratios of the interladder coupling $B_{\text{inter}}^{\text{O-O}}$ with $B_{\text{leg}}^{\text{Cu-O}}$, $B_{\text{intra}}^{\text{O-O}}$, and $B_{\text{leg}}^{\text{O-O}}$ against the O leg charge density $\langle n_{O_L} \rangle$ at different Δ_{dp}, for comparison against the pressure dependence of ρ_a/ρ_c. Increasing $B_{\text{inter}}^{\text{O-O}}/B_{\text{leg}}^{\text{Cu-O}}$ and $B_{\text{inter}}^{\text{O-O}}/B_{\text{intra}}^{\text{O-O}}$ with increasing $\langle n_{O_L} \rangle$ does simulate the decreasing ρ_a/ρ_c with pressure [17]. The increases are small within the positive Δ_{dp} region compared to the factor of 4–5 decrease in ρ_a/ρ_c in SCCO between ambient pressure and $P = 3.5$–4.5 GPa at $T \sim 50$ K. The insets of Fig. 5(b) show schematically the 2D checkerboard O sublattices obtained upon ignoring the Cu ions. The diagonal bonds in the checkerboard lattice are due to the reduced intraladder leg n.n.n. O-O bonds. The dramatic changes in the slopes of all bond orders at $\Delta_{dp} = -1$ are due to a quantum phase transition from the lattice on the left with n.n.n. O-O bonds stronger than the n.n. O-O bonds to the lattice on the right with stronger n.n. O-O bonds. The simultaneous changes in the slopes in all three ratios at $\Delta_{dp} = -1$ is a signature of discrete jump in Cu-ion ionicity from nearly +2 to nearly +1. Figure S7 [41] shows the corresponding plots for $t'_{pp} = 0.3$. The behavior is very similar to that in Figs. 5(a) and 5(b). *We conclude that the large decrease in ρ_a/ρ_c necessarily requires transition from positive to negative Δ_{dp}.*

IV. DISCUSSION AND CONCLUSIONS

A. Consequences of valence transition

It is instructive to estimate the charge density on the ladder oxygen sites following the valence transition. Within one formula unit of SCCO, 10 Cu and 20 O atoms compose the

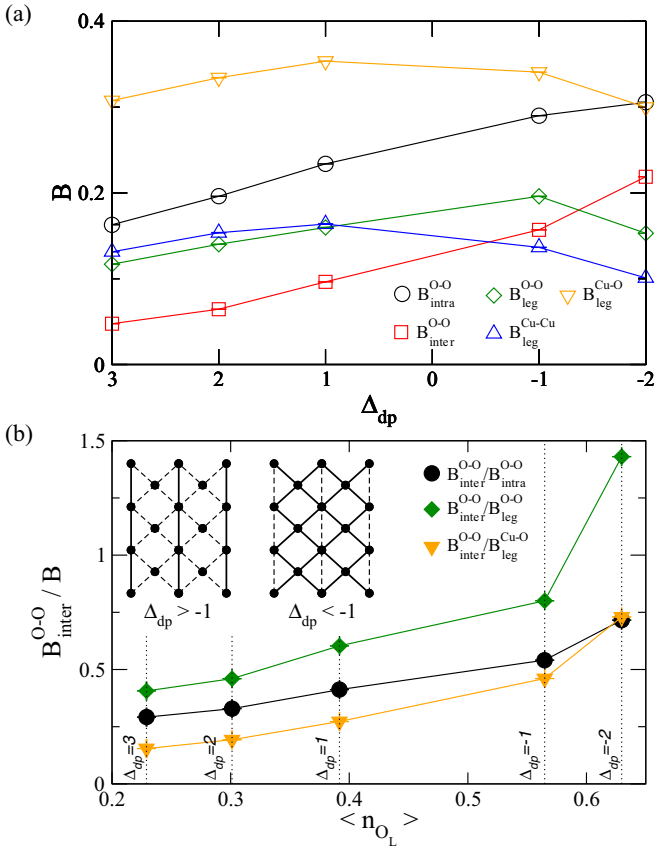

FIG. 5. (a) Bond orders for $\delta = 0.125$ and $t'_{pp} = 0.5$ versus Δ_{dp}. (b) Ratios of interladder bond order with all intraladder bond orders, versus hole density on the oxygen ions occupying the interior legs of the coupled ladder. Calculations are for the 12×2 coupled ladder. Results for $t'_{pp} = 0.3$ are nearly identical and are shown in Figs. S7(a) and S7(b). The inset shows the effective checkerboard O sublattice for positive (left) versus negative (right) charge-transfer gap (see text).

CuO_2 chains, and 14 Cu and 21 O atoms the Cu_2O_3 ladders. Assuming ionic charges Sr^{2+}/Ca^{2+}, Cu^{2+}, and O^{2-}, 6 holes per formula unit must be added for charge neutrality. Under the pressure required for SC, approximately 4 holes occupy the ladders [55]. Following the valence transition we assume that the Cu and O in the chains remain Cu^{2+} and O^{2-}, and that the charge on Cu in the ladders is not precisely integral but in the range of $+1.3$ to $+1.5$. With these assumptions, the average ladder oxygen charge is -1.3 to -1.5, which is close to a $\frac{1}{4}$-filled band of holes ($\frac{3}{4}$-filled band of electrons). There occurs an enhancement of superconducting correlations by Hubbard U uniquely at or very close $\frac{1}{4}$-filling in 2D in the presence of sufficiently strong frustrations [3,64].

The valence transition model may seem too exotic to be relevant to real cuprates. However, cuprates share a common feature with all negative charge-transfer gap compounds discovered so far; viz., *the key cation in one of two possible charged states in every case is either exactly closed-shell or exactly half-filled once crystal field effects are taken into consideration (see the Appendix).* This commonality [27,28,30–33], hitherto unnoticed (see, however, discussions in Chaps. 4 and 5 of Ref. [65]), is also shared by heavy-fermion systems in which valence instability has been most commonly found: the electronic configurations of the final states of the valence transitions $Yb^{3+} \rightarrow Yb^{2+}$ or from $Ce^{3+} \rightarrow Ce^{4+}$ are both closed shell. Coming back to SCCO, universal 2D resistivity [17] and gapless spin excitations [19,34,35,37] in the pressure-driven metallic state preceding SC are not only naturally expected when nearly all the charge carriers are on the 2D O sublattice but also they are difficult to understand within any other scenario.

B. Implications for two-dimensional cuprates

A pressure-induced valence transition in SCCO has consequential implications for the layered 2D cuprates where a similar transition has been proposed under doping [22] and whose normal state remains mysterious even after intense research through decades. This is a topic of ongoing research, but we point out that qualitative understanding of seemingly widely different kinds of experiments, which are difficult to understand within the standard one- or multiband Hubbard models, become available within the valence transition theory. A partial list of such experiments along with their possible explanations within the valence transition theory follows.

(i) A sudden jump in the charge-carrier density from δ to $1 + \delta$ is found in hole-doped layered cuprates at a quantum critical doping at low temperatures in the presence of magnetic field that destroys SC [66]. A similar jump occurs in the electron-doped cuprates with the carrier density $1 - \delta$ following the transition [67]. The mechanisms of these phase transitions are currently not understood [66,68,69]. Within the valence transition theory, there occurs dopant-induced change in Cu ionicity in both cases that generates a 2D oxygen hole band. With the assumption of complete integer Cu-valence transition from $+2$ to $+1$, hole densities of precisely $1 + \delta$ in the hole-doped materials and $1 - \delta$ in the electron-doped materials are expected.

(ii) A charge-ordered (CO) phase within the pseudogap phase is ubiquitous to hole-doped cuprates, and a similar CO phase has also been seen in the electron-doped cuprates. The CO phase does not occur in the antiferromagnetic region, and while the CO periodicity can be somewhat arbitrary in the weakly hole-doped materials, the periodicity saturates to a commensurate value $4a_0$ at or near a critical hole-doping concentration (here a_0 is the unit cell dimension) [70,71]. It is broadly accepted that CO is driven by many-electron interactions and not nesting. Within neither the single-band nor the multiband Hubbard model for cuprates can a physical explanation for this specific periodicity be found. Within the valence transition theory, post valence transition charge carriers occupy entirely the O band, which is $\frac{1}{4}$-filled. In previous work, we have shown that precisely at this carrier concentration there is a strong tendency to electron correlation-driven transition to a paired-electron crystal (PEC), which is a period 4 charge-ordered state of spin-singlet pairs [72,73].

(iii) Multiple research groups have hypothesized that SC in hole-doped cuprates emerges from the strange metallic state that occupies the region between the quantum critical doping at which the pseudogap vanishes at zero temperature and the doping at which the SC ends [66,74,75]. The strange metal state has been discussed also in the context of electron-doped

cuprates [67,76]. It has further been claimed that in the hole-doped systems the strange metal phase evolves from the CO phase [77] and that charge carriers in the strange metallic state of $YBa_2Cu_3O_7$ may be charge $2e$ bosons [78,79]. As of now there is no simple explanation within the standard models for cuprates for these closely related observations. Within the valence transition theory, both the strange metal and SC can evolve from the PEC. The evolution from the PEC to a $\frac{1}{4}$-filled frustrated metal with spin-paired charge carriers, and from the latter to the superconducting state, is a distinct possibility that merits further investigation [3,64].

(iv) The disappearance of Cu nuclear-quadrupole-resonance line splittings in electron-doped materials beyond critical doping indicates a state with a very small electric field gradient [80,81]. The latter is expected for Cu^{1+} ions with symmetric $3d^{10}$ configuration [22].

C. Experimental prediction

We end this paper with an experimental prediction: pressure-dependent Hall coefficient measurements in SCCO will find a large jump in the number of charge carriers beyond P_c, exactly as in the layered systems beyond critical doping [66,67].

ACKNOWLEDGMENTS

Work at the University of Arizona was supported by the National Science Foundation (NSF) Grant No. NSF-CHE-1764152. Some calculations in this work were supported under Project No. TG-DMR190068 of the Extreme Science and Engineering Discovery Environment (XSEDE), which is supported by National Science Foundation Grant No. ACI-1548562. Specifically, we used the Bridges2 system at the Pittsburgh Supercomputing Center, which is supported by NSF Award No. ACI-1928147. Other calculations were performed using the High Performance Computing (HPC) resources supported by the University of Arizona.

APPENDIX: NEGATIVE CHARGE-TRANSFER GAP AND CATION IONIZATION ENERGY, A CONSISTENT PATTERN

Theories of transition metal compounds, especially oxides, usually assume that the ligand anions are overwhelmingly closed shell in the undoped state (O^{2-} in oxides) and only a few of the anions are charged in the doped state (O^{1-}). The concept of negative charge-transfer gap, that the energy of charge transfer from ligand to metal can be negative, and that even in the undoped state anions can be overwhelmingly open shell, is antithetical to this traditional idea even though this possibility was included in the classic paper by Zaanen, Sawatzky, and Allen [82]. Computational works that that have found negative charge-transfer gap in different systems [27–30,32,33] are based on many-body corrections to band theoretical approaches (LSDA + U, DFT + DMFT, and QMC). The theories correctly emphasize that the primary requirements for a negative charge-transfer gap are that the formal oxidation state of the transition metal cation must be large, and covalency effects are strong relative to the charge-transfer gap. Our approach to negative charge-transfer agrees with these requirements, but goes a step further by pointing out a common characteristic shared by the metal cation in nearly all negative charge-transfer compounds, viz., the cation in the lower charged-state is either exactly closed shell or *exactly half-filled once crystal structure effects are taken into consideration* [83]. These are precisely when ionization to the next higher charged states can be energetically expensive. In Sec. S.5, in Fig. S6(a) we reproduce our previous plot of the fourth ionization energies of Pb, Bi, and Po, neighboring elements in the periodic table. The closed-shell electron configuration of Bi^{3+} is behind its relatively high ionization energy. Figure S6(b) shows a similar plot for the fourth ionization energy of $3d$ transition elements. The local peak at Fe^{3+} is due to its half-filled d^5 electron occupancy. Negative charge-transfer gaps in $BaBiO_3$ [32] and FeO_2 [28,30] are ascribed to these higher-than-usual ionization energies in the state with the lower cation charge.

For d-electron occupancies less than five crystal structure effects become relevant. For CrO_2, as was noted correctly by Korotin *et al.* [27], a formal oxidation state of Cr^{4+} with two electrons occupying two of the t_{2g} orbitals would have led to Mott-insulating behavior. Based on LSDA + U calculations the authors found nearly pure $2p$ electrons from the oxygen anions to cross the Fermi level in this material, with d-d Coulomb repulsion playing a minimal role. This is also anticipated within our ionic model, within which with octahedral anion arrangement the Cr^{3+} electron configuration is half-filled and therefore very stable, and the overall oxygen charge is -1.5, exactly what is found [30] in FeO_2. Finally the stability of closed-shell Au^{1+} explains the negative charge-transfer in $AuTe_2$ [29]. There exists then a consistent pattern among most negative charge-transfer compounds.

[1] M. Qin, C.-M. Chung, H. Shi, E. Vitali, C. Hubig, U. Schollwöck, S. R. White, and S. Zhang, Absence of superconductivity in the pure two-dimensional Hubbard model, Phys. Rev. X **10**, 031016 (2020).

[2] M.-S. Vaezi, A.-R. Negari, A. Moharramipour, and A. Vaezi, Amelioration for the sign problem: An adiabatic quantum Monte Carlo algorithm, Phys. Rev. Lett. **127**, 217003 (2021).

[3] N. Gomes, W. W. De Silva, T. Dutta, R. T. Clay, and S. Mazumdar, Coulomb enhanced superconducting pair correlations in the frustrated quarter-filled band, Phys. Rev. B **93**, 165110 (2016).

[4] S. Jiang, D. J. Scalapino, and S. R. White, Ground-state phase diagram of the t-t'-J model, Proc. Natl. Acad. Sci. U.S.A. **118**, e2109978118 (2021).

[5] Y.-F. Jiang, T. P. Devereaux, and H.-C. Jiang, Ground state phase diagram and superconductivity of the doped Hubbard model on six-leg square cylinders, arXiv:2303.15541.

[6] X. Lu, J.-X. Zhang, S.-S. Gong, D. N. Sheng, and Z.-Y. Weng, Sign structure in the square-lattice t-t'-J model and numerical consequences, arXiv:2303.13498.

[7] S. Jiang, D. J. Scalapino, and S. R. White, Pairing properties of the t-t'-t''-J model, Phys. Rev. B **106**, 174507 (2022).

[8] H. Xu, C.-M. Chung, M. Qin, U. Schollwöck, S. R. White, and S. Zhang, Coexistence of superconductivity with partially filled stripes in the Hubbard model, arXiv:2303.08376.

[9] Y. Gannot, Y.-F. Jiang, and S. A. Kivelson, Hubbard ladders at small U revisited, Phys. Rev. B **102**, 115136 (2020).

[10] H.-C. Jiang and S. A. Kivelson, Stripe order enhanced superconductivity in the Hubbard model, Proc. Natl. Acad. Sci. USA **119**, e2109406119 (2022).

[11] E. Dagotto, Experiments on ladders reveal a complex interplay between a spin-gapped normal state and superconductivity, Rep. Prog. Phys. **62**, 1525 (1999).

[12] K. Le Hur and T. M. Rice, Superconductivity close to the Mott state: From condensed-matter systems to the superfluidity in optical lattices, Ann. Phys. **324**, 1452 (2009).

[13] E. Dagotto, J. Riera, and D. Scalapino, Superconductivity in ladders and coupled planes, Phys. Rev. B **45**, 5744 (1992).

[14] R. M. Noack, N. Bulut, D. J. Scalapino, and M. G. Zacher, Enhanced $d_{x^2-y^2}$ pairing correlations in the two-leg Hubbard ladder, Phys. Rev. B **56**, 7162 (1997).

[15] M. Dolfi, B. Bauer, S. Keller, and M. Troyer, Pair correlations in doped Hubbard ladders, Phys. Rev. B **92**, 195139 (2015).

[16] M. Uehara, T. Nagata, J. Akimitsu, H. Takahashi, N. Mori, and K. Kinoshita, Superconductivity in the ladder material $Sr_{0.4}Ca_{13.6}Cu_{24}O_{41.84}$, J. Phys. Soc. Jpn. **65**, 2764 (1996).

[17] T. Nagata, M. Uehara, J. Goto, J. Akimitsu, N. Motoyama, H. Eisaki, S. Uchida, H. Takahashi, T. Nakanishi, and N. Mori, Pressure-induced dimensional crossover and superconductivity in the hole-doped two-leg ladder compound $Sr_{14-x}Ca_xCu_{24}O_{41}$, Phys. Rev. Lett. **81**, 1090 (1998).

[18] K. M. Kojima, N. Motoyama, H. Eisaki, and S. Uchida, The electronic properties of cuprate ladder materials, J. Electron Spectrosc. Relat. Phenom. **117-118**, 237 (2001).

[19] T. Vuletić, B. Korin-Hamzić, T. Ivek, S. Tomić, B. G. M. Dressel, and J. Akimitsu, The spin-ladder and spin-chain system $(La,Y,Sr,Ca)_{14}Cu_{24}O_{41}$: Electronic phases, charge and spin dynamics, Phys. Rep. **428**, 169 (2006).

[20] J.-P. Song, S. Mazumdar, and R. T. Clay, Absence of Luther-Emery superconducting phase in the three-band model for cuprate ladders, Phys. Rev. B **104**, 104504 (2021).

[21] J.-P. Song, S. Mazumdar, and R. T. Clay, Doping asymmetry in the three-band Hamiltonian for cuprate ladder: Failure of the standard model of superconductivity in cuprates, Phys. Rev. B **107**, L241108 (2023).

[22] S. Mazumdar, Valence transition model of the pseudogap, charge order, and superconductivity in electron-doped and hole-doped copper oxides, Phys. Rev. B **98**, 205153 (2018).

[23] I. Felner and I. Nowik, First-order valence phase transition in cubic $Yb_xIn_{1-x}Cu_2$, Phys. Rev. B **33**, 617 (1986).

[24] C. Dallera, M. Grioni, A. Shukla, G. Vanko, J. L. Sarrao, J. P. Rueff, and D. L. Cox, New spectroscopy solves an old puzzle: The Kondo scale in heavy fermions, Phys. Rev. Lett. **88**, 196403 (2002).

[25] K. Miyake, New trend of superconductivity in strongly correlated electron systems, J. Phys.: Condens. Matter **19**, 125201 (2007).

[26] K. Miyake and S. Watanabe, Ubiquity of unconventional phenomena associated with critical valence fluctuations in heavy fermion metals, Philos. Mag. **97**, 3495 (2017).

[27] M. A. Korotin, V. I. Anisimov, D. I. Khomskii, and G. A. Sawatzky, CrO_2: A self-doped double exchange ferromagnet, Phys. Rev. Lett. **80**, 4305 (1998).

[28] S. S. Streltsov, A. O. Shorikov, S. L. Skornyakov, A. I. Poteryaev, and D. I. Khomskii, Unexpected 3+ valence of iron in FeO_2, a geologically important material lying "in between" oxides and peroxides, Sci. Rep. **7**, 13005 (2017).

[29] S. V. Streltsov, V. V. Roizenc, A. V. Ushakova, A. R. Oganov, and D. I. Khomskii, Old puzzle of incommensurate crystal structure of calaverite $AuTe_2$ and predicted stability of novel AuTe compound, Proc. Natl. Acad. Sci. U.S.A. **115**, 9945 (2018).

[30] E. Koemets, I. Leonov, M. Bykov, E. Bykova, S. Chariton, G. Aprilis, T. Fedotenko, S. Clement, J. Rouquette, J. Haines, V. Cerantola, K. Glazyrin, C. McCammon, V.B. Prakapenka, M. Hanfland, H.P. Liermann, V. Svitlyk, R. Torchio, A.D. Rosa, T. Irifune *et al.*, Revealing the complex nature of bonding in the binary high-pressure compound FeO_2, Phys. Rev. Lett. **126**, 106001 (2021).

[31] V. Bisogni, S. Catalano, R. J. Green, M. Gibert, R. Scherwitzl, Y. Huang, V. N. Strocov, P. Zubko, S. Balandeh, J.-M. Triscone, G. Sawatzky, and T. Schmitt, Ground-state oxygen holes and the metal-insulator transition in the negative charge-transfer rare-earth nickelates, Nat. Commun. **7**, 13017 (2016).

[32] A. Khazraie, K. Foyevtsova, I. Elfimov, and G. A. Sawatzky, Oxygen holes and hybridization in the bismuthates, Phys. Rev. B **97**, 075103 (2018).

[33] M. C. Bennett, G. Hu, G. Wang, O. Heinonen, P. R. C. Kent, J. T. Krogel, and P. Ganesh, Origin of metal-insulator transition in correlated perovskite metals, Phys. Rev. Res. **4**, L022005 (2022).

[34] N. Fujiwara, N. Mori, Y. Uwatoko, T. Matsumoto, N. Motoyama, and S. Uchida, Superconductivity of the $Sr_2Ca_{12}Cu_{24}O_{41}$ spin-ladder system: Are the superconducting pairing and the spin-gap formation of the same origin? Phys. Rev. Lett. **90**, 137001 (2003).

[35] N. Fujiwara, Y. Fujimaki, S. Uchida, K. Matsubayashi, T. Matsumoto, and Y. Uwatoko, NMR and NQR study of pressure-induced superconductivity and the origin of critical-temperature enhancement in the spin-ladder cuprate $Sr_2Ca_{12}Cu_{24}O_{41}$, Phys. Rev. B **80**, 100503(R) (2009).

[36] T. Pang, Universal critical normal sheet resistance in ultrathin films, Phys. Rev. Lett. **62**, 2176 (1989).

[37] H. Mayaffre, P. Auban-Senzier, M. Nardone, D. Jérome, D. Poilblanc, C. Bourbonnais, U. Ammerahl, G. Dhalenne, and A. Revcolevschi, Absence of a spin gap in the superconducting ladder compound $Sr_2Ca_{12}Cu_{24}O_{41}$, Science **279**, 345 (1998).

[38] M. Isobe, T. Ohta, M. Onoda, F. Izumi, S. Nakano, J. Q. Li, Y. Matsui, E. Takayama-Muromachi, T. Matsumoto, and H. Hayakawa, Structural and electrical properties under high pressure for the superconducting spin-ladder system $Sr_{0.4}Ca_{13.6}Cu_{24}O_{41+\delta}$, Phys. Rev. B **57**, 613 (1998).

[39] Y. Piskunov, D. Jérome, P. Auban-Senzier, P. Wzietek, and A. Yakubovsky, Hole redistribution in $Sr_{14-x}Ca_xCu_{24}O_{41}$ ($x = 0$, 12) spin ladder compounds: ^{63}Cu and ^{17}O NMR studies under pressure, Phys. Rev. B **72**, 064512 (2005).

[40] M. Bugnet, S. Loeffler, D. Hawthorn, H. A. Dabkowska, G. M. Luke, P. Schattschneider, G. A. Sawatzky, G. Radtke, and G. A. Botton, Real-space localization and quantification of hole dis-

tribution in chain-ladder $Sr_3Ca_{11}Cu_{24}O_{41}$ superconductor, Sci. Adv. **2**, e1501652 (2016).

[41] See Supplemental Material at http://link.aps.org/supplemental/10.1103/PhysRevB.108.134510 for details of the DMRG calculations, DMRG truncation error and finite-size extrapolations, data for alternate parameter values, and plots of ionization energies.

[42] E. M. Stoudenmire and S. R. White, Real-space parallel density matrix renormalization group, Phys. Rev. B **87**, 155137 (2013).

[43] M. Fishman, S. R. White, and E. M. Stoudenmire, The ITensor software library for tensor network calculations, SciPost Phys. Codebases **4**, 1 (2022).

[44] T. F. A. Müller, V. Anisimov, T. M. Rice, I. Dasgupta, and T. Saha-Dasgupta, Electronic structure of ladder cuprates, Phys. Rev. B **57**, R12655 (1998).

[45] M. Hirayama, Y. Yamaji, T. Misawa, and M. Imada, *Ab initio* effective Hamiltonians for cuprate superconductors, Phys. Rev. B **98**, 134501 (2018).

[46] J. B. Torrance, J. E. Vazquez, J. J. Mayerle, and V. Y. Lee, Discovery of a neutral-to-ionic phase transition in organic materials, Phys. Rev. Lett. **46**, 253 (1981).

[47] J. B. Torrance, A. Girlando, J. J. Mayerle, J. I. Crowley, V. Y. Lee, P. Batail, and S. J. LaPlaca, Anomalous nature of neutral-to-ionic phase transition in tetrathiafulvalene-chloranil, Phys. Rev. Lett. **47**, 1747 (1981).

[48] J. Hubbard and J. B. Torrance, Model of the neutral-ionic phase transformation, Phys. Rev. Lett. **47**, 1750 (1981).

[49] S. Koshihara, Y. Tokura, T. Mitani, G. Saito, and T. Koda, Photoinduced valence instability in the organic molecular compound tetrathiafulvalene-*p*-chloranil (TTF-CA), Phys. Rev. B **42**, 6853 (1990).

[50] M. Masino, N. Castagnetti, and A. Girlando, Phenomenology of the neutral-ionic valence instability in mixed stack charge-transfer crystals, Crystals **7**, 108 (2017), and references therein.

[51] Y. Ohta, T. Tohyama, and S. Maekawa, Charge-transfer gap and superexchange interaction in insulating cuprates, Phys. Rev. Lett. **66**, 1228 (1991).

[52] J. E. Hirsch, Effect of orbital relaxation on the band structure of cuprate superconductors and implications for the superconductivity mechanism, Phys. Rev. B **90**, 184515 (2014).

[53] N. Barisic and D. K. Sunko, High-T_c cuprates: a story of two electronic subsystems, J. Supercond. Novel Magn. **35**, 1781 (2022).

[54] M. Azuma, Z. Hiroi, M. Takano, K. Ishida, and Y. Kitaoka, Observation of a spin gap in $SrCu_2O_3$ comprising spin-$\frac{1}{2}$ quasi-1D two-leg ladders, Phys. Rev. Lett. **73**, 3463 (1994).

[55] Y. Piskunov, D. Jérome, P. Auban-Senzier, P. Wzietek, C. Bourbonnais, U. Ammerhal, G. Dhalenne, and A. Revcolevschi, $(Sr/Ca)_{14}Cu_{24}O_{41}$ spin ladders studied by NMR under pressure, Eur. Phys. J. B **24**, 443 (2001).

[56] S. Frank, A. Huber, U. Ammerahl, M. Hücker, and C. A. Kuntscher, Polarization-dependent infrared reflectivity study of $Sr_{2.5}Ca_{11.5}Cu_{24}O_{41}$ under pressure: Charge dynamics, charge distribution, and anisotropy, Phys. Rev. B **90**, 224516 (2014).

[57] Y. Mizuno, T. Tohyama, and S. Maekawa, Electronic states of doped spin ladders $(Sr,Ca)_{14}$ $Cu_{24}O_{41}$, J. Phys. Soc. Jpn. **66**, 937 (1997).

[58] J. D. Gale, GULP–a computer program for the symmetry adapted simulation of solids, JCS Faraday Trans. **93**, 629 (1997).

[59] J. D. Gale and A. L. Rohl, The general utility lattice program, Mol. Simul. **29**, 291 (2003).

[60] J. D. Gale, Empirical potential derivation for ionic materials, Philos. Mag. B **73**, 3 (1996).

[61] J. D. Gale, GULP: Capabilities and prospects, Z. Kristallogr. **220**, 552 (2005).

[62] E. M. McCarron, III, M. A. Subramanian, J. C. Calabrese, and R. L. Harlow, The incommensurate structure of $Sr_{14-x}Ca_xCu_{24}O_{41}$ $(0 < x \sim 8)$ a superconductor byproduct, Mater. Res. Bull. **23**, 1355 (1988).

[63] B. D. E. McNiven, J. P. F. LeBlanc, and G. T. Andrews, Optical constants of crystalline $Bi_2Sr_2CaCu_2O_{8+\delta}$ by Brillouin light scattering, Supercond. Sci. Technol. **34**, 065005 (2021).

[64] W. W. De Silva, N. Gomes, S. Mazumdar, and R. T. Clay, Coulomb enhancement of superconducting pair-pair correlations in a $\frac{3}{4}$-filled model for κ-$(BEDT\text{-}TTF)_2X$, Phys. Rev. B **93**, 205111 (2016).

[65] D. I. Khomskii, *Transition Metal Compounds* (Cambridge University, Cambridge, England, 2014).

[66] C. Proust and L. Taillefer, The remarkable underlying ground states of cuprate superconductors, Annu. Rev. Condens. Matter Phys. **10**, 409 (2019).

[67] R. L. Greene, P. R. Mandal, N. R. Poniatowski, and T. Sarkar, The strange metal state of the electron-doped cuprates, Annu. Rev. Condens. Matter Phys. **11**, 213 (2020).

[68] J. He *et al.*, Fermi surface reconstruction in electron-doped cuprates without antiferromagnetic long-range order, Proc. Natl. Acad. Sci. U.S.A. **116**, 3449 (2019).

[69] P. R. Mandal, T. Sarkar, and R. L. Greene, Anomalous quantum criticality in the electron-doped cuprates, Proc. Natl. Acad. Sci. U.S.A. **116**, 5991 (2019).

[70] A. Mesaros, K. Fujita, S. D. Edkins, M. H. Hamidian, H. Eisaki, S. Uchida, J. C. S. Davis, M. J. Lawler, and E.-A. Kim, Commensurate $4a_0$ period charge density modulations throughout the $Bi_2Sr_2CaCu_2O_{8+x}$ pseudogap regime, Proc. Natl. Acad. Sci. U.S.A. **113**, 12661 (2016).

[71] H. Lu, M. Hashimoto, S. D. Chen, S. Ishida, D. Song, H. Eisaki, A. Nag, M. Garcia-Fernandez, R. Arpaia, G. Ghiringhelli, L. Braicovich, J. Zaanen, B. Moritz, K. Kummer, N. B. Brookes, K. J. Zhou, Z. X. Shen, T. P. Devereaux, and W. S. Lee, Identification of a characteristic doping for charge order phenomena in Bi-2212 cuprates via RIXS, Phys. Rev. B **106**, 155109 (2022).

[72] H. Li, R. T. Clay, and S. Mazumdar, The paired-electron crystal in the two-dimensional frustrated quarter-filled band, J. Phys.: Condens. Matter **22**, 272201 (2010).

[73] S. Dayal, R. T. Clay, H. Li, and S. Mazumdar, Paired electron crystal: Order from frustration in the quarter-filled band, Phys. Rev. B **83**, 245106 (2011).

[74] A. Legros, S. Bernhabib, W. Tabis, F. Laliberté, M. Dion, M. Lizaire, D. Vignolles, H. Raffy, Z. Z. Li, P. Auban-Senzier, N. Doiron-Leyraud, P. Fournier, D. Colson, L. Taillefer, and C. Proust, Universal T-linear resistivity and Planckian dissipation in overdoped cuprates, Nat. Phys. **15**, 142 (2019).

[75] P. W. Phillips, N. E. Hussey, and P. Abbamonte, Stranger than metals, Science **377**, eabh4273 (2022).

[76] T. Sarkar, N. R. Poniatowski, J. S. Higgins, P. R. Mandal, M. K. Chan, and R. L. Greene, Hidden strange metallic state in underdoped electron-doped cuprates, Phys. Rev. B **103**, 224501 (2021).

[77] G. Seibold, R. Arpaia, Y. Y. Peng, R. Fumagalli, L. Braicovich, C. D. Castro, M. Grilli, G. C. Ghiringhelli, and S. Caprara, Strange metal behaviour from charge density fluctuations in cuprates, Commun. Phys. **4**, 7 (2021).

[78] C. Yang, Y. Liu, Y. Wang, L. Feng, Q. He, J. Sun *et al.*, Intermediate bosonic metallic state in the superconductor-insulator transition, Science **366**, 1505 (2019).

[79] C. Yang, H. Liu, Y. Liu, J. Wang, D. Qiu, S. Wang, Y. Wang, Q. He, X. Li, P. Li, Y. Tang, J. Wang, X. C. Xie, J. M. Valles, Jr., J. Xiong, and Y. Li, Signatures of a strange metal in a bosonic system, Nature **601**, 205 (2022).

[80] M. Abe, K. Kumagai, S. Awaji, and T. Fujita, Cu-NMR studies of $Nd_{2-x}Ce_xCuO_{4-\gamma}$, Phys. C (Superconduct.) **160**, 8 (1989).

[81] M. Jurkutat, D. Rybicki, O. P. Sushkov, G. V. M. Williams, A. Erb, and J. Haase, Distribution of electrons and holes in cuprate superconductors as determined from ^{17}O and ^{63}Cu nuclear magnetic resonance, Phys. Rev. B **90**, 140504(R) (2014).

[82] J. Zaanen, G. A. Sawatzky, and J. W. Allen, Band gaps and electronic structure of transition-metal compounds, Phys. Rev. Lett. **55**, 418 (1985).

[83] S. Mazumdar, Negative charge-transfer gap and even parity superconductivity in Sr_2RuO_4, Phys. Rev. Res. **2**, 023382 (2020).